

A bifunctional oxygen electrocatalyst from monodisperse MnCo_2O_4 nanoparticles on nitrogen enriched carbon nanofibers†

Cite this: *RSC Adv.*, 2014, 4, 25089Received 6th February 2014
Accepted 27th May 2014

DOI: 10.1039/c4ra01037j

www.rsc.org/advances

Chaohe Xu,^{ab} Meihua Lu,^a Yi Zhan^a and Jim Yang Lee^{*a}

Monodisperse MnCo_2O_4 nanoparticles supported on nitrogen enriched carbon nanofibers (NCF) exhibited synergetic component interactions that resulted in higher ORR and OER activities than commercial Pt/C catalysts.

The higher theoretical energy densities of metal-air batteries are their most noticeable advantage over lithium-ion batteries for electric vehicle propulsion applications. For rechargeability, the oxygen reduction reaction (ORR) and the oxygen evolution reaction (OER) in the cathode must have high electrochemical reversibility. These reactions are however kinetically challenged necessitating the presence of bifunctional oxygen electrocatalysts equally adept at ORR and OER.¹ Although noble metals have shown excellent electrocatalytic activities (e.g. Pt for ORR and RuO_2 or IrO_2 for OER) in aqueous solution, their scarcity and high cost are deployment challenges.^{2,3} The interest to develop low cost alternatives to the noble metals is clear and vital.

Mixed-valence transition metal oxides with a spinel structure have been used as bifunctional oxygen electrocatalysts in alkaline solutions. Among them those based on cobalt oxides have drawn the most potential because of reasonably good electrocatalytic activity, low cost, ease of preparation and good chemical stability. The ORR and OER electrocatalytic activities could be increased further by partially substituting the cobalt ions with Ni and Mn ions.⁴ Despite these improvements, the ternary oxides still could not match the performance of Pt-based catalysts. For example, at an ORR current density of $\sim 3 \text{ mA cm}^{-2}$ (the current density measured at the half-wave potential of 20 wt% Pt/C at 5 mV s^{-1}), the oxygen reduction potentials were

0.49, 0.59 and 0.68 V (vs. RHE) for Co_3O_4 , Co_2MnO_4 and a $\text{Co}_3\text{O}_4\text{-Co}_2\text{MnO}_4$ composite respectively, significantly more negative than the 0.80 V for Pt/C. The limiting current densities of oxygen reduction on these oxides were also lower than that of Pt/C.⁵ In a different study, while Pt nanoparticles on carbon nanotubes could deliver 125 mA cm^{-2} at a loading of only 0.1 mg cm^{-2} , MnCo_2O_4 had to be loaded to 14 mg cm^{-2} on carbon black to yield a current density of 300 mA cm^{-2} .⁶ Clearly the mass catalytic activity of oxide-based electrocatalysts leaves plenty of room for improvement. Recent reports have shown that hybrid structures of oxides and carbon nanofoams could improve the application performance through synergistic interactions if there is strong coupling between the components. For instance, the Dai group covalently bonded Co_3O_4 and MnCo_2O_4 nanoparticles to graphene and reported oxygen electrocatalytic activities higher than those of Co_3O_4 , MnCo_2O_4 or graphene alone. The activities were comparable to that of Pt/C and more stable than the later in KOH solution.^{7,8}

In a separate development, hetero-atom doped nanocarbons were also found to be highly ORR active. For instance, nitrogen-doped carbon nanotube arrays have shown higher electrocatalytic activity and greater chemical stability than Pt on carbon for ORR under alkaline conditions.⁹ Pt supported on nitrogen-doped carbon also surpassed Pt on pristine carbon in ORR performance.¹⁰ Research over the years has ratified the ORR activity of nitrogen-doped carbon where the N-C-N bonding motifs are the most likely active sites.^{11–13} In particular nitrogen doping of graphitic carbon lattices (graphitic-N) forms one of the most active ORR catalytic sites by facilitating the electron transfer from the carbon conduction band to the anti-bonding orbitals of oxygen.^{14,15} However, graphitic-N is not as easily formed as pyridinic and pyrrolic-N by direct nitrogen doping because of a higher energy of formation. A better strategy is to start with precursors which can introduce more graphitic-N in the nanocarbon; for which nitrogen-containing conducting polymers are good choices.¹⁶ For example, polypyrrole (PPy) has been used to produce microporous nanocarbon with graphitic-N to pyridinic-N ratios as high as 5.89.¹⁷

^aDepartment of Chemical and Biomolecular Engineering, National University of Singapore, 10 Kent Ridge Crescent, Singapore 119260, Singapore. E-mail: cheleejy@nus.edu.sg; Fax: +65-67791936; Tel: +65-65162899

^bDepartment of Mechanical Engineering, National University of Singapore, 9 Engineering Drive 1, Singapore 117576, Singapore

† Electronic supplementary information (ESI) available: Additional TEM, XDR, XPS and LSV curves. See DOI: 10.1039/c4ra01037j

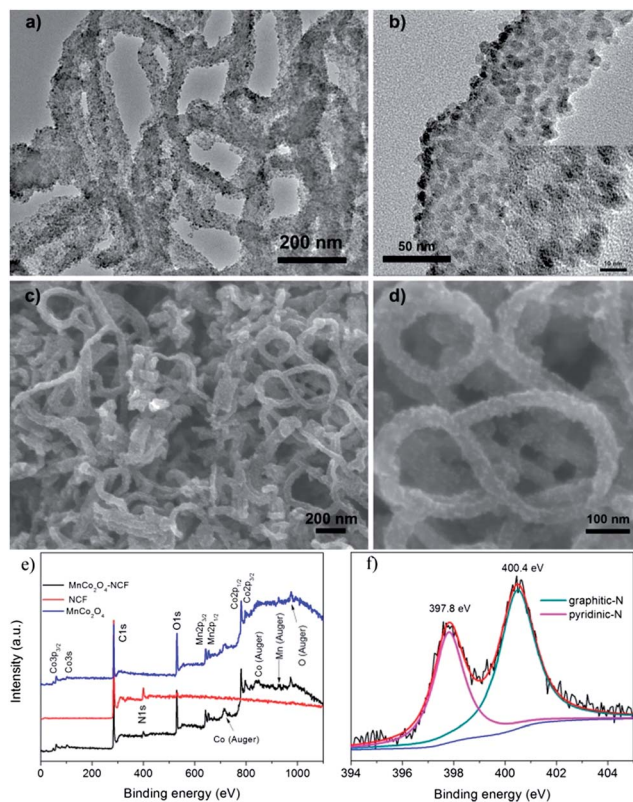


Fig. 1 (a and b) TEM and (c and d) SEM images of the MnCo₂O₄-NCF composite; (e) XPS spectrum of NCFs (red), MnCo₂O₄-NCF composite (black), and pure MnCo₂O₄ nanoparticles (blue); (f) N1s spectrum of NCFs.

Based on these background information we have developed a MnCo₂O₄ nanoparticle-nitrogen enriched carbon nanofiber (NCF) composite with an ORR performance as good as the commercial Pt/C catalyst; and an OER performance which is even better. The composite was prepared by a solvothermal method (see experimental details in ESI†), using nitrogen enriched carbon nanofibers which were derived from pyrolysis of PPy nanowires (40–60 nm in diameters, see Fig. S1†) in nitrogen at 800 °C for 2 h. In a typical preparation, Mn and Co precursors in a ratio of Mn-Co = 1 : 2, ammonia solution; and H₂O were added to a NCF suspension in ethanol. After ageing at 80 °C for several hours, the suspension was solvothermally treated at 150 °C and the final product was recovered by centrifugation. As shown in the typical TEM and SEM images of Fig. 1, there was uniform deposition of 2–4 nm nanoparticles on the surface of the NCFs, which were about 40–60 nm in diameter and several μm in length (Fig. S2†). All the peaks in the X-ray diffraction (XRD) patterns of the composite indexed well with the MnCo₂O₄ spinel structure (Fig. S3†). The HRTEM image in the inset of Fig. 1b also shows that the MnCo₂O₄ nanoparticles were highly crystalline. The MnCo₂O₄ loading in the NCFs was ~35 wt% according to thermal analysis (Fig. S4†). Scanning transmission electron microscopy (STEM) analysis of elemental distribution in the composite (Fig. 2) measured homogeneity of Mn, Co, N and O distributions throughout the

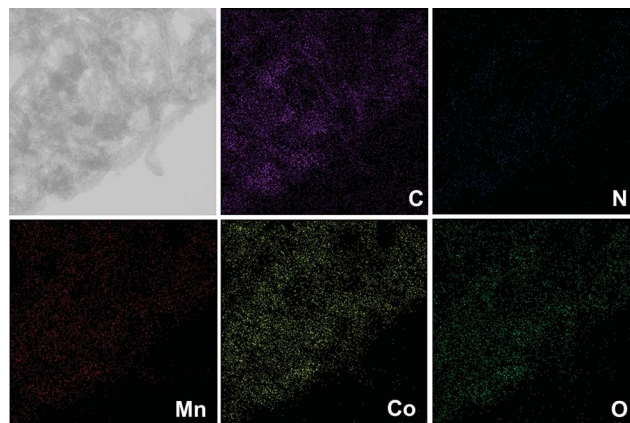


Fig. 2 Elemental mapping images of C, N, Mn, Co and O.

composite. Hence it may be concluded that the MnCo₂O₄ nanoparticles had uniformly decorated the NCF.

X-ray photoelectron spectroscopy (XPS) of the NCFs and their composite (Fig. 1e and f) confirmed the presence of N in very high amounts (~11.5 at.%). The N1s spectrum of NCF could be deconvoluted into two components (Fig. 1f) representing pyridinic-N (397.8 eV) and graphitic-N (400.4 eV) respectively. The graphitic-N content calculated as such was as high as 54.6%. Such a high graphitic-N content, when compounded with MnCo₂O₄ nanoparticles which have previously shown bifunctional electrocatalytic activities for oxygen,¹⁸ may result in a greater oxygen electrocatalysis performance through improvements in the charge transfer process and in electron conduction through the catalyst system. The Co-Mn ratio of ~2 as measured by XPS was in good agreement with the starting precursor ratio. High resolution XPS also revealed the interaction between MnCo₂O₄ nanoparticles and NCF. Relative to pure MnCo₂O₄, there was a general decrease in the O1s, Mn2p_{3/2} and Co2p_{3/2} binding energies for the MnCo₂O₄-NCF composite (Fig. S5†). The pyridinic-N1s (398.1 eV) and graphitic-N1s (400.7 eV) peaks of the composite were ~0.3 eV higher than those in NCF (Fig. S6a and b†); while the C1s peak of the composite was shifted to slightly lower binding energy (Fig. S7†). Collectively these are indications of electron migrations from the NCF to metal oxide nanoparticles; and from the nitrogen lone pair to the sp² carbon skeleton.⁷ There was therefore strong electronic interaction between MnCo₂O₄ and NCF in the composite. Such interaction could render the oxide nanoparticles more conducting and more electrochemically active than a binary mixture of NCF and MnCo₂O₄ nanoparticles.

For the MnCo₂O₄-NCF composite, Fig. S6c and d† also show an asymmetric O1s peak which could be deconvoluted into two distinguishable peaks at 529.9 and 531.1 eV (530.2 and 531.5 eV respectively for MnCo₂O₄) which correspond well with lattice oxygen and surface adsorbed oxygen-containing species (possibly hydroxide or water).¹⁹ The higher relative intensity and integrated peak area of adsorbed oxygen species on the composite may be used to suggest a stronger oxygen affinity in the former, which predisposes the composite to oxygen electrocatalysis.

The ORR performance of MnCo_2O_4 -NCF composite was evaluated by cyclic voltammetry on a glassy carbon electrode in O_2 - or N_2 -saturated 0.1 M KOH solutions. Unsupported MnCo_2O_4 nanoparticles (with comparable sizes of 3–5 nm, Fig. S8†) and NCFs were also evaluated under the same conditions for comparison. Fig. 3a shows the cyclic voltammograms (CVs) of various samples together with a standard commercial Pt/C catalyst (40 wt% Pt on graphitized carbon, Aldrich). The MnCo_2O_4 -NCF composite exhibited a more positive ORR onset potential (-0.08 V vs. Ag/AgCl) and a higher cathodic peak current than those of MnCo_2O_4 nanoparticles and NCFs, suggesting a synergy of functions after the component integration. The composite was more similar to Pt/C where the onset potential was about -0.06 V. The ORR kinetics was also measured by a rotating-disk electrode in O_2 -saturated 0.1 M KOH solution. Fig. 3b shows the typical linear sweep voltammograms (LSVs) of MnCo_2O_4 -NCF composite. The Koutecky–Levich plots were all linear and parallel to one another, confirming first-order reaction kinetics. The electron transfer numbers (n) calculated from the slopes in the limited current region (-0.4 to -0.6 V, Fig. 3c) were ~ 3.96 . These measurements indicate that MnCo_2O_4 nanoparticles supported on NCFs are effective for a 4-electron ORR. By comparison the electron transfer numbers of NCFs, VC-72 carbon, and physical mixtures of MnCo_2O_4 with NCFs; and of MnCo_2O_4 with VC-72 carbon; were 2.45, 2.16, 3.64, and 2.30 respectively (Fig. S9†). The electron transfer number was higher in the NCF mixture than in the VC-mixture because the higher intrinsic ORR activity of the NCFs provided a better match with the intrinsic activity of MnCo_2O_4 . The LSVs of the composite, various control samples, and of Pt/C, are compared in Fig. 2d. The current density of the composite was higher than that of Pt/C in the mixed-controlled and diffusion-controlled potential regions. The half-wave potential of MnCo_2O_4 -NCF was also slightly more positive than

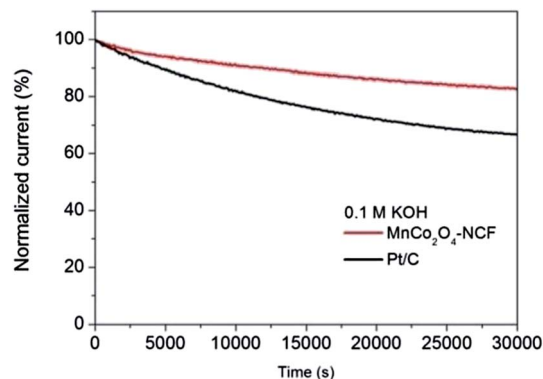


Fig. 4 Chronoamperograms of MnCo_2O_4 -NCF and Pt/C on GC electrodes at -0.4 V (vs. Ag/AgCl) in O_2 -saturated 0.1 M KOH solution.

Pt/C (-0.21 V compared with -0.23 V for Pt/C). More importantly the MnCo_2O_4 -NCF composite was very stable in 0.1 M KOH, where the 17% decrease of ORR activity after 30 000 s of continuous operation at -0.4 V compares favourably with the 34% decrease on Pt/C (Fig. 4). Hence the MnCo_2O_4 -NCF composite surpasses Pt/C in both the activity and stability of ORR.

The OER performance of the MnCo_2O_4 -NCF composite was also measured, by extending the anodic potential limit to 1.0 V (Fig. 5a). In a 0.1 M KOH solution, OER occurred earlier (at less positive potentials) on the MnCo_2O_4 -NCF and current densities were also generally higher than those of Pt/C and NCFs. The onset potential of OER on MnCo_2O_4 -NCF was about 0.6 V. While the OER catalytic properties of MnCo_2O_4 -NCF are superior to Pt/C, they are still below the performance of precious metal oxides (RuO_2 or IrO_2) which are the best OER catalysts for commercial electrolysis.^{20,21} In order to evaluate the overall suitability of MnCo_2O_4 -NCF as a bifunctional oxygen electrocatalyst, we used the difference between the half-wave potential of ORR on Pt/C and the potential for water electrolysis at 10 mA cm^{-2} as an indicator. The smaller the difference, the closer is the catalyst to being truly bifunctional. The value was 1.04 V for the MnCo_2O_4 -NCF composite; which is smaller than previous results.⁵ The difference cannot be measured for Pt/C (black curves) and NCFs (red curves) with OER potentials lower than 1.0 V (Fig. 5a). The composite stability under the OER condition was evaluated by CV. Fig. 5b shows that the current density

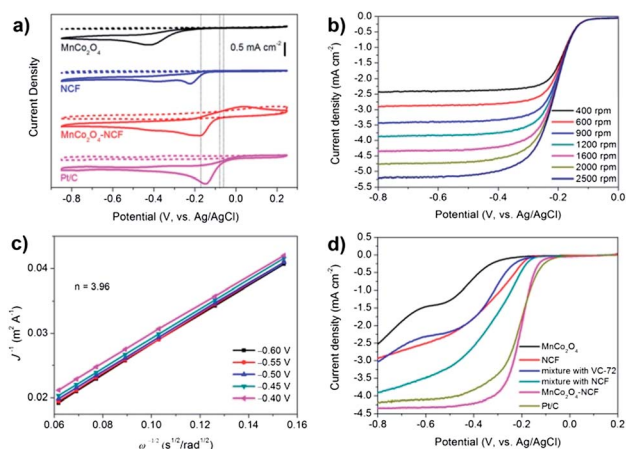


Fig. 3 Electrochemical performance of the MnCo_2O_4 -NCF composite as an ORR catalyst. (a) CV of MnCo_2O_4 , NCF, MnCo_2O_4 -NCF, and Pt/C on GC electrodes in O_2 -saturated or N_2 -saturated 0.1 M KOH. (b) LSV of MnCo_2O_4 -NCF composite at 5 mV s^{-1} . (c) The corresponding Koutecky–Levich plots of MnCo_2O_4 -NCF composite at different potentials. (d) LSV of MnCo_2O_4 -NCF and various controls at 5 mV s^{-1} and a rotation speed of 900 rpm.

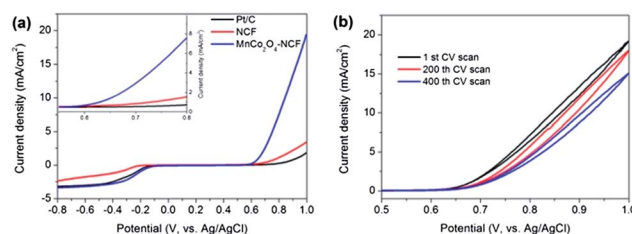


Fig. 5 (a) Suitability of MnCo_2O_4 -NCF as a bifunctional catalyst for ORR and OER in comparison with NCF and Pt/C. (b) CV curves recorded at 1st cycle, 100th cycle, and 400th cycle for MnCo_2O_4 -NCF composites. Rotation speed = 900 rpm.

decreased to $\sim 15 \text{ mA cm}^{-2}$ after 400 cycles. The retention of only 83.3% of the initial current density indicates that improvements are needed to increase the OER stability of this material.

In summary, we have prepared a MnCo_2O_4 nanoparticle-nitrogen enriched carbon nanofiber composite with an ORR performance as good as the standard commercial Pt/C catalyst and an even better OER performance. The improved electrochemical performance correlated well with the abundance of ORR-active graphitic-N sites in NCFs, and the effective integration of MnCo_2O_4 nanoparticles and nitrogen enriched carbon nanofibers to synergize charge transfer and post-charge transfer electron conduction. The use of conducting polymer-derived carbon nanostructures with a high nitrogen content as an active support for non-precious metal catalysts should be explored further for the preparation of low-cost bifunctional oxygen electrocatalysts.

Acknowledgements

This research is financially supported by the research grant (R-265-000-436-305) of Advanced Energy Storage Programme from the SERC, Singapore.

Notes and references

- 1 F. Y. Cheng and J. Chen, *Chem. Soc. Rev.*, 2012, **41**, 2172–2192.
- 2 S. Guo, D. Li, H. Zhu, S. Zhang, N. M. Markovic, V. R. Stamenkovic and S. Sun, *Angew. Chem., Int. Ed.*, 2013, **52**, 3465–3468.
- 3 S. J. Guo and S. H. Sun, *J. Am. Chem. Soc.*, 2012, **134**, 2492–2495.
- 4 Y. Liang, Y. Li, H. Wang and H. Dai, *J. Am. Chem. Soc.*, 2013, **135**, 2013–2036.
- 5 D. Wang, X. Chen, D. G. Evans and W. Yang, *Nanoscale*, 2013, **5**, 5312–5315.
- 6 F. Bidault, D. J. L. Brett, P. H. Middleton and N. P. Brandon, *J. Power Sources*, 2009, **187**, 39–48.
- 7 Y. Y. Liang, H. L. Wang, J. G. Zhou, Y. G. Li, J. Wang, T. Regier and H. J. Dai, *J. Am. Chem. Soc.*, 2012, **134**, 3517–3523.
- 8 Y. Liang, Y. Li, H. Wang, J. Zhou, J. Wang, T. Regier and H. Dai, *Nat. Mater.*, 2011, **10**, 780–786.
- 9 K. Gong, F. Du, Z. Xia, M. Durstock and L. Dai, *Science*, 2009, **323**, 760–764.
- 10 F. B. Su, Z. Q. Tian, C. K. Poh, Z. Wang, S. H. Lim, Z. L. Liu and J. Y. Lin, *Chem. Mater.*, 2010, **22**, 832–839.
- 11 T. P. Fellinger, F. Hasche, P. Strasser and M. Antonietti, *J. Am. Chem. Soc.*, 2012, **134**, 4072–4075.
- 12 J. D. Wiggins-Camacho and K. J. Stevenson, *J. Phys. Chem. C*, 2011, **115**, 20002–20010.
- 13 H. Kim, K. Lee, S. I. Woo and Y. Jung, *Phys. Chem. Chem. Phys.*, 2011, **13**, 17505–17510.
- 14 J. Xu, G. Dong, C. Jin, M. Huang and L. Guan, *ChemSusChem*, 2013, **6**, 493–499.
- 15 P. Wang, Z. Wang, L. Jia and Z. Xiao, *Phys. Chem. Chem. Phys.*, 2009, **11**, 2730–2740.
- 16 G. Wu, N. H. Mack, W. Gao, S. G. Ma, R. Q. Zhong, J. T. Han, J. K. Baldwin and P. Zelenay, *ACS Nano*, 2012, **6**, 9764–9776.
- 17 F. Su, C. K. Poh, J. S. Chen, G. Xu, D. Wang, Q. Li, J. Lin and X. W. Lou, *Energy Environ. Sci.*, 2011, **4**, 717–724.
- 18 H. L. Wang, Y. Yang, Y. Y. Liang, G. Y. Zheng, Y. G. Li, Y. Cui and H. J. Dai, *Energy Environ. Sci.*, 2012, **5**, 7931–7935.
- 19 F. Y. Cheng, J. A. Shen, B. Peng, Y. D. Pan, Z. L. Tao and J. Chen, *Nat. Chem.*, 2011, **3**, 79–84.
- 20 T. Reier, M. Oezaslan and P. Strasser, *ACS Catal.*, 2012, **2**, 1765–1772.
- 21 W. Hu, Y. Q. Wang, X. H. Hu, Y. Q. Zhou and S. L. Chen, *J. Mater. Chem.*, 2012, **22**, 6010–6016.